Science of the Total Environment 686 (2019) 1164–1172

Contents lists available at ScienceDirect

Science of the Total Environment

journal homepage: www.elsevier.com/locate/scitotenv

Experimental influence of storm-surge salinity on soil greenhouse gas emissions from a tidal salt marsh

Margaret Capooci, Josep Barba, Angelia L. Seyfferth, Rodrigo Vargas *

Department of Plant and Soil Sciences, University of Delaware, 152 Townsend Hall, 531 South College Ave., Newark, DE 19716, USA

HIGHLIGHTS

- Studied the influence a pulse-change in salinity on salt marsh GHG biogeochemistry
- Coupled automated GHG measurements with pore water chemistry
- CO_2 decreased with decreased salinity; CH_4, and N_2O fluxes increased.
- Salt marsh soils recovered from salinity changes relatively quickly.

GRAPHICAL ABSTRACT

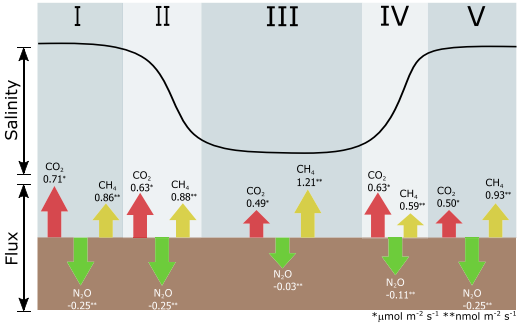

ARTICLE INFO

Article history:
Received 18 March 2019
Received in revised form 31 May 2019
Accepted 2 June 2019
Available online 04 June 2019

Editor: Jay Gan

Keywords:
Carbon cycle
Biogeochemistry
Extreme events
Automated measurements

ABSTRACT

Storm surges can substantially alter the water level and salinity in tidal salt marshes. Little is known about how changes experienced during storm surges affect greenhouse gas emissions (GHG; CO_2, CH_4, N_2O) from tidal salt marsh soils. Understanding how storm surges influence ecosystem processes is critical for evaluating the ecosystem's sensitivity to sea level rise. To explore how hurricane-induced changes in salinity affect GHG emissions, we exposed intact soil mesocosms (0–9 cm depth) from a Mid-Atlantic temperate salt marsh to pulse changes in salinity experienced at the site before, during, and after Hurricane Joaquin in 2015. Soil temperature, oxygen, and water level were kept constant to avoid confounding effects throughout the experiment. Automated measurements (hourly resolution) of soil GHG emissions were recorded in control (i.e., no salinity changes) and treatment mesocosms, and combined with soil pore water chemistry (i.e., SO_4^{2-}, S^{2-}, Fe^{2}, TN_b, redox potential, pH) to characterize the biogeochemical responses. Using mixed effects models, we found that the role of different biogeochemical processes, such as sulfur cycling, changed throughout the experiment, underscoring the complex nature of GHG emissions in tidal salt marsh soils. Overall, soils subjected to a salinity decrease had greater GHG emissions than control soils, which were maintained at 17 ppt. The treatment soils had a 24% and 23% increase in global warming potential (20- and 100-year scenarios, respectively) indicating that storm surges can produce pulses of GHG emissions. However, both CH_4 and N_2O emissions returned to baseline values (following hysteresis responses) when initial conditions were reestablished. The results support the fact that tidal salt marshes are resilient ecosystems, as soil GHG emissions recovered relatively quickly from the pulse event.

* Corresponding author at: 152 Townsend Hall, 531 South College Ave., Newark, DE 19716, USA.
E-mail addresses: mcapooci@udel.edu (M. Capooci), jbarba@udel.edu (J. Barba), angelias@udel.edu (A.L. Seyfferth), rvargas@udel.edu (R. Vargas).

https://doi.org/10.1016/j.scitotenv.2019.06.032
0048-9697/

1. Introduction

Tidal salt marshes provide a wide variety of ecosystem services, including reactive nitrogen removal and carbon storage (Jordan et al., 2011; Valiela and Teal, 1979). Carbon stored in these ecosystems, along with mangrove forests and seagrass beds, is termed "blue carbon" and has become a topic of global interest. In the United States, wetlands cover 44.6 million hectares, with 2.6 million (5.8%) of the total comprised of salt marshes (Dahl, 2011; Dahl and Stedman, 2013). Despite their small area, salt marshes can sequester C at high rates with an average of 218 ± 24 g C m^{-2} yr^{-1} (McLeod et al., 2011). Blue carbon research typically focuses on quantifying C stocks and assessing how they will change under various climate change scenarios. However, there is also a need to quantify baselines for a wide range of greenhouse gas (GHG; CO_2, CH_4, N_2O) emissions and to ascertain how these fluxes are influenced by weather changes, particularly by pulse events (Crooks et al., 2011; McLeod et al., 2011).

According to the Intergovernmental Panel on Climate Change (IPCC), coastal systems will likely experience shifts in the frequency and/or intensity of storm events. For example, while hurricane frequency is not expected to change (Wong et al., 2014), storm intensity is likely to increase, with higher wind speeds and precipitation rates. Furthermore, the IPCC found that storm surges increased in the past 48 years, likely due to sea level rise (IPCC, 2014). Therefore, there is increased potential for storm surges and flooding from both terrestrial and oceanic storm events in coastal areas (IPCC, 2014). Thus, there is a critical need to assess how salt marsh GHG emissions respond to the salinity and tidal inundation shifts caused by hurricanes. These data may be useful for predicting how these ecosystems will respond to changing weather conditions and future climate scenarios.

In tidal salt marshes, CO_2 emissions from soils (i.e., soil CO_2 efflux) ranges from 240 to 720 g C m^{-2} y^{-1} and arises from a variety of processes, including autotrophic respiration and decomposition of organic matter via aerobic and anaerobic microorganisms (i.e. heterotrophic respiration) (Tobias and Neubauer, 2019). Due to the flooded soil conditions of tidal salt marshes, anaerobic respiration dominates. The most energetically-favorable electron acceptor, O_2, gets used rapidly near the soil surface. As a result, facultative anaerobic or strict anaerobic microorganisms use other electron acceptors, including NO_3^-, Fe^3, SO_4^{2-}, and even CO_2, to produce GHGs (Ponnamperuma, 1972). Furthermore, as salinity changes, the proportion of various ions changes as well. Higher salinity water has higher levels of SO_4^{2-} due to greater ocean water inputs, which changes the proportions of available electron acceptors in anaerobic soils and the amount of CO_2 emitted. For example, if a storm event decreases the salinity of the marsh, there is the potential for a decrease in SO_4^{2-} availability, which may result in a decrease in CO_2 emissions (Chambers et al., 2013) and an increase in CH_4 emissions (Capone and Kiene, 1988). Therefore, there is a pressing need to provide information regarding how changes in salinity influence soil CO_2 and CH_4 efflux rates in salt marshes.

While wetlands do not contribute significantly to global CO_2 emissions, they are the largest natural source of CH_4 to the atmosphere (IPCC, 2000). CH_4 has a global warming potential 25 times that of CO_2 (Forster et al., 2007). In North America, freshwater wetlands emit CH_4 at a rate of 36.0 ± 5.0 g C m^{-2} yr^{-1}, while salt marshes emit CH_4 at a much lower rate of 3.6 ± 5.0 g C m^{-2} yr^{-1} (Bridgham et al., 2006). Salinity is a major control on CH_4 emissions in salt marshes, with higher salinity generally resulting in lower emissions (Poffenbarger et al., 2011). It is thought that the limited amount of CH_4 released from salt marshes is due to methanogens being outcompeted for electron donors by SO_4^{2-} and Fe^3 reducers (Furukawa et al., 2004; King and Wiebe, 1978). Storm events can change the salinity of the water in tidal salt marshes on a short time-scale, causing an increase or decrease of CH_4 depending on proportion of freshwater to oceanic inputs during the flooding stage. Accordingly, these pulse events might result in changes in short-term emission of CH_4 in tidal salt marshes.

In addition to CO_2 and CH_4, wetlands also emit small quantities of N_2O, which has a global warming potential 298 times that of CO_2 (Forster et al., 2007). However, wetlands can become small sinks of N_2O (Audet et al., 2014; Jørgensen and Elberling, 2012; Schaufler et al., 2010). The production and consumption of N_2O in wetlands appears to be strongly influenced by water level and its effect on O_2 availability in the soil (Davidson, 1991; Jørgensen and Elberling, 2012; Kliewer and Gilliam, 1995; Martikainen et al., 1993). N_2O production is more likely to occur during low levels of O_2 (Liikanen and Martikainen, 2003); however, depending on the conditions of the soil (i.e., gas transport properties, N_2O consumption rate, water level), the N_2O may be converted to N_2 or consumed before it gets emitted to the atmosphere (Chapuis-Lardy et al., 2007; Clough et al., 2005; Heincke and Kaupenjohann, 1999). Additionally, salinity has been shown to inhibit complete denitrification, potentially allowing for a build-up of N_2O (Inubushi et al., 1999; Menyailo et al., 1997). If a storm event lowers salinity levels, in addition to flooding the soils, there will likely be less build-up of N_2O in the soils due to less inhibition of complete denitrification. However, to the best of our knowledge, only one study has investigated the effects of storm events on N_2O production and consumption in tidal salt marshes (Diefenderfer et al., 2018).

For this study, we conducted a mesocosm experiment that simulated a decrease in salinity associated with a hurricane-induced storm surge event that was dominated by freshwater precipitation inputs. We used an automated system to continuously measure CO_2, CH_4, and N_2O emissions from soil mesocosms to obtain high temporal data resolution (hourly basis) and coupled these measurements with pore water chemical analyses. We hypothesized that: a) emissions of all three GHGs would increase with decreasing salinity due to less inhibition (i.e. more favorable redox conditions due to reduced SO_4^{2-} concentrations) on the biogeochemical processes that produce the GHGs; and b) the temporal pattern of GHG emissions would respond to the salinity regime and the subsequent shifts in potential biogeochemical pathways, such as sulfur and iron reduction.

2. Materials and methods

2.1. Study site and soil collection

Soil cores were collected from St. Jones Reserve, a subsection of the Delaware National Estuarine Research Reserve located near Dover, Delaware (39°05″ N, 75°26″ W). The site comprises mostly of a tidal salt marsh with salinities typically in the mesohaline range (5–18 ppt) (DNREC, 1999). The marsh is connected to the Atlantic Ocean via the St. Jones River and the Delaware Bay. Dominant plant species within the marsh include *Spartina alterniflora, Spartina patens,* and *Spartina cynosuroides*. The marsh soils are classified as a silty clay loam (10% sand, 61% silt, and 29% clay) as measured by the University of Delaware's Soil Testing Lab.

2.2. Mesocosms flow-through incubation

Six intact soil cores (i.e., mesocosms; 20 cm in diameter, 9 cm deep) were collected within a 1 × 1 m area near a tidal creek to ensure the mesocosms were as similar to each other as possible. Mesocosms were collected in January 2017 within a PVC collar, fixed to a polyethylene board, and sealed with duct tape to prevent soil and water loss during transport to the laboratory using previously reported methods (Northrup et al., 2018; Petrakis et al., 2017a). River water from the St. Jones River and Murderkill River (both <5 km from where the soils where collected), which differ in salinity (8.2 ± 1.8 ppt and 27.2 ± 1.1 ppt, respectively), was used to maintain continuously flooded conditions and to manipulate salinity levels during the experiment.

The experiment was designed to simulate salinity patterns observed during storm surges, such as the one produced by Hurricane Joaquin in 2015 at the site (Fig. 1a), when the water level in the tidal creek

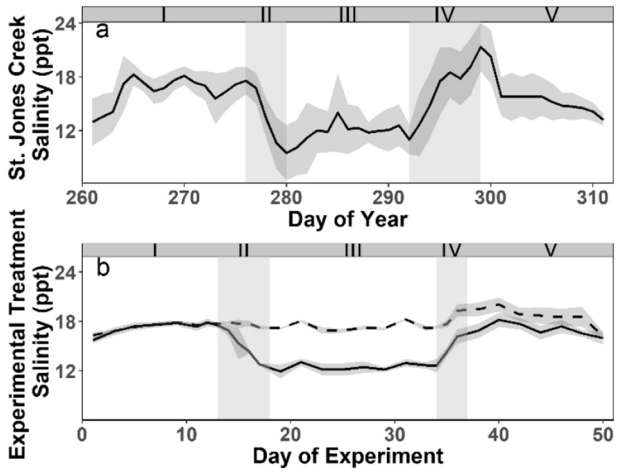

Fig. 1. (a) Average daily salinity values before, during, and after Hurricane Joaquin's storm surge at St. Jones Reserve, Dover, DE in 2015 (NOAA National Estuarine Research Reserve System (NERRS), 2015). (b) Average daily experimental control (dashed line) and treatment (solid line) salinity data. In both graphs, shading denotes ±1 SD. Salinity data at the study site was collected using a YSI 6600 (Yellow Springs, Ohio) probe.

increased due to a combination of oceanic storm surge and freshwater rain inputs. As a result, the water (i.e., a mix of costal ocean and rain water sources) overtopped the creek banks and flooded the high marsh, which typically does not flood during high tides. The salinity in the tidal creek changed as well. The salinity decreased during the storm surge from 17 ppt to 12 ppt and remained stable for 12 days, before increasing again back to 17 ppt. The experiment was designed to replicate the salinity changes in the creek and was divided into five phases to capture GHG and pore water changes before, during, and shortly after the pulse event. The five phases were: I – 17 ppt, II – 17 to 12 ppt, III – 12 ppt, IV – 12 to 17 ppt, and V – 17 ppt. Three mesocosms received the experimental treatment, while three replicate mesocosms served as controls, maintaining a salinity of 17 ppt, the average high tide salinity in the St. Jones River in 2015 (NOAA National Estuarine Research Reserve System (NERRS), 2015).

For each mesocosm, we designed a flow-through system where water was pumped on top of the mesocosm (at a flow rate of 1.05 mL/min) and out the bottom of the mesocosm (at a flow rate of 0.89 mL/min) using a peristaltic pump (Golander BT100s, Norcross, Georgia). The water table was maintained at 2 cm above the soil surface to replicate the flooded conditions during the storm surge. Salinity was changed by changing the proportions of the higher salinity Murderkill River water and the lower salinity St. Jones River water at predetermined points during the experiment. The outflow tubing was capped with a 100 μm nylon mesh to minimize soil loss. The flow-through system was designed to maintain hydrological connectivity and flooded conditions for the duration of the experiment. Soil temperature was maintained at a constant 22 °C to avoid confounding effects.

Each soil mesocosm was instrumented with a soil moisture probe (Li-COR 8150–202, Lincoln, Nebraska) and a soil temperature sensor (Li-COR 8150–203, Lincoln, Nebraska). Oxygen sensors (Fibox 4, PreSens, Germany) were instrumented in three randomly selected mesocosms (1 control, 2 treatment mesocosms) to confirm that anoxic conditions were kept throughout the experiment. Additionally, a Rhizon sampler (Eikjelkamp, The Netherlands) was inserted into the soil of each mesocosm at a 45° angle for pore water collection using previously described methods (Seyfferth and Fendorf, 2012).

2.3. Greenhouse gas flux measurement and calculation

Greenhouse gas (GHG; CO_2, CH_4, N_2O) fluxes were measured in each soil mesocosm once per hour for the duration of the experiment using automated chambers (Li-COR 8100–104, Lincoln, Nebraska) coupled with both a closed-path infrared gas analyzer (LI-8100A, Li-COR, Lincoln, Nebraska) and a cavity ring-down spectrometer (Picarro G2508, Santa Clara, California) as described in previous studies (Petrakis et al., 2017a, 2017b). For each flux observation, gas concentrations were measured every second for 3 min. Fluxes were calculated using Soil Flux Pro (v4.0: Li-COR, Lincoln, Nebraska) following the quality assurance and quality control protocol established in Petrakis et al. (2017b), with the following modification: if CO_2 fluxes had an $R^2 > 0.90$, we considered the micrometeorological conditions inside the chambers were stable enough for calculating the fluxes and the measurements for all three gases were kept. Measurements that did not meet this threshold were marked as not-a-number (NaN).

2.4. Soil pore water extraction and analysis

Soil pore water (~20 mL) was extracted every other day during Phase I, III, and V, and every day during Phase II and IV when salinity changes in treatment mesocosms were rapid. Pore water was collected into vials that were previously purged with N_2 and crimp sealed in an anaerobic glove bag (95% N_2/5% H_2). For all samples, salinity, pH, redox potential, sulfide, and ferrous iron were measured as described in Northrup et al. (2018). Sulfate was measured using a Dionex DX-500 (Sunnyvale, California). Additionally, TN_b was measured using an Elementar Vario-TOC Cube (Elementar Americas, Mount Laurel, New Jersey). TN_b measures a variety of dissolved nitrogen compounds, such as ammonia, nitrites, and nitrates.

2.5. Data analyses

Daily, hourly, and by phase flux averages were calculated for each gas for both the control and the treatment mesocosms. Averages are reported as mean ± SD. The Mann-Whitney *U* test was used to test for differences between the treatment and the control for each phase of the experiment.

Mixed effects models using daily data for each mesocosm were run on each experimental phase for each of the three gases to analyze the relationships between the gas fluxes and the pore water variables (salinity, pH, redox, sulfide, sulfate, ferrous iron, TN_b). Only variables and ecologically relevant first-order interactions were included in the saturated model to eliminate potential spurious correlations. Temperature, soil water content, and oxygen concentration were not included in the models because they were constant throughout the experiment. Prior to running the analyses, all variables were centered and scaled to improve the model's performance and to simplify the interpretation of the results (Gelman and Hill, 2007). The variance inflation factor (VIF) was tested for each model to ascertain if there were collinearity between variables and their interactions. If VIF >3 for a variable and/or an interaction, we removed that variable from the model (Zuur et al., 2010). We included mesocosm identification in the random part of the model in order to account for temporal autocorrelation between measurements. For each gas and phase, we evaluated all possible models combining predictor variables and relevant first-order interactions in order to achieve the minimum adequate model in terms of the corrected Akaike Information Criterion (AICc). The AICc accounts for model overfitting. The best model was reported in the results.

The global warming potential (GWP), which converts the cumulative radiative forcing capacity of CH_4 and N_2O to CO_2 equivalents, was calculated by multiplying the cumulative daily sums (g m^2 day^{-1}) of the control and treatment emissions by their respective 20 and 100 year GWP scenarios (86 and 34 for CH_4, 268 and 298 for N_2O, respectively) to convert them into CO_2 equivalencies ($CO_{2\text{-eq}}$) (Myhre et al., 2013). We report the 20 and 100 year GWP in $CO_{2\text{-eq}}$ for each GHG flux as a practice to account for ranges in carbon-climate feedbacks (Petrakis et al., 2017b).

All analyses were carried out using R 3.4.3 (R Foundation for Statistical Computing, Vienna, Austria). Mixed effects models were

performed using the R *nlme* package (Pinheiro et al., 2018) and model selection and comparison was done with the R *MuMIn* package (Barton, 2018).

3. Results

3.1. Experimental conditions

The salinity regime for the treatment mesocosms closely resembled the salinity changes that occurred during the Hurricane Joaquin storm surge (Fig. 1). Soils were constantly flooded, so soil oxygen levels were low, averaging 0.02 ± 0.16% throughout the experiment. The volumetric water content of the mesocosms was 0.42 ± 0.01 m^3/m^3. The soil temperature was 21.4 ± 0.5 °C.

3.2. Soil greenhouse gas fluxes

CO_2 fluxes for the treatment and the control were similar throughout the first three phases of the experiment (Figs. 2a, 3a). By Phase IV, the CO_2 emissions from the treatment mesocosms were significantly higher than the control and remained so in Phase V ($p = 0.03$, $p < 0.001$, Fig. 3a). Fig. 2a shows a noticeable increase in treatment CO_2 emissions beginning at the end of Phase III and continuing midway through Phase V, which is reflected by the darker red colors in the heat maps (Fig. 2b, c).

CH_4 fluxes from the treatment mesocosms were more variable than the control mesocosms, particularly when the salinity decreased and remained low during Phases II and III and right after the increase of salinity in Phase IV (Fig. 2d). In Phases I, III, IV, and V, the treatment mesocosms had significantly higher emissions than the control soils ($p = 0.005$, $p < 0.001$, $p = 0.03$, $p < 0.001$, Fig. 3b).

N_2O fluxes for both the control and the treatment mesocosms showed similar patterns and values throughout the experiment, with the treatment fluxes slightly increasing during Phases II, III, and IV, before declining back towards the control fluxes in Phase V (Fig. 2g, i). The treatment was significantly different from the control in Phases IV and V ($p = 0.05$, $p = 0.04$, Fig. 3c). For most of the experiment, the soils were sinks of N_2O, but in Phase III, both the control and the treatment mesocosms became sources of N_2O (Fig. 2g, h). Means by phase for each mesocosm are presented in Supplementary Fig. 1.

3.3. Soil pore water

Salinity was significantly different between the control and the treatment for Phases III (17.4 ± 0.5 ppt vs 12.4 ± 0.4 ppt, $p < 0.001$), IV (17.9 ± 1.0 ppt vs 14.0 ± 1.7 ppt, $p < 0.001$), and V (18.6 ± 1.2 ppt vs 17.0 ± 0.8 ppt, $p = 0.03$) (Fig. 3d). Redox (Fig. 3e), pH, and sulfide were not significantly different between control and treatment mesocosms for all phases of the experiment (Table S1). While sulfide did not show significant differences between the treatment and the control, SO_4^{2-} was significantly higher in the control than the treatment in Phases III (306.9 ± 23.4 mg/L vs 206.9 ± 5.0 mg/L, $p < 0.001$) and V (316.6 ± 18.9 mg/L vs 260.0 ± 68.3 mg/L, $p = 0.001$) (Fig. 3f). For both the treatment and the control, Fe^2 concentrations increased as the experiment went on, with the treatment having significantly higher Fe^2 concentrations during Phases IV (11.8 ± 1.3 mg/L vs 15.3 ± 2.1 mg/L, $p = 0.05$) and V (14.5 ± 4.9 mg/L vs 21.9 ± 6.7 mg/L, $p = 0.05$) (Fig. 3g). The TN_b concentrations were similar between control and treatment for most of the experiment, except in Phase IV, when the treatment had significantly higher concentrations than the control (3.33 ± 0.2 mg/L vs ± 3.72 ± 0.2, $p = 0.03$, Fig. 3h).

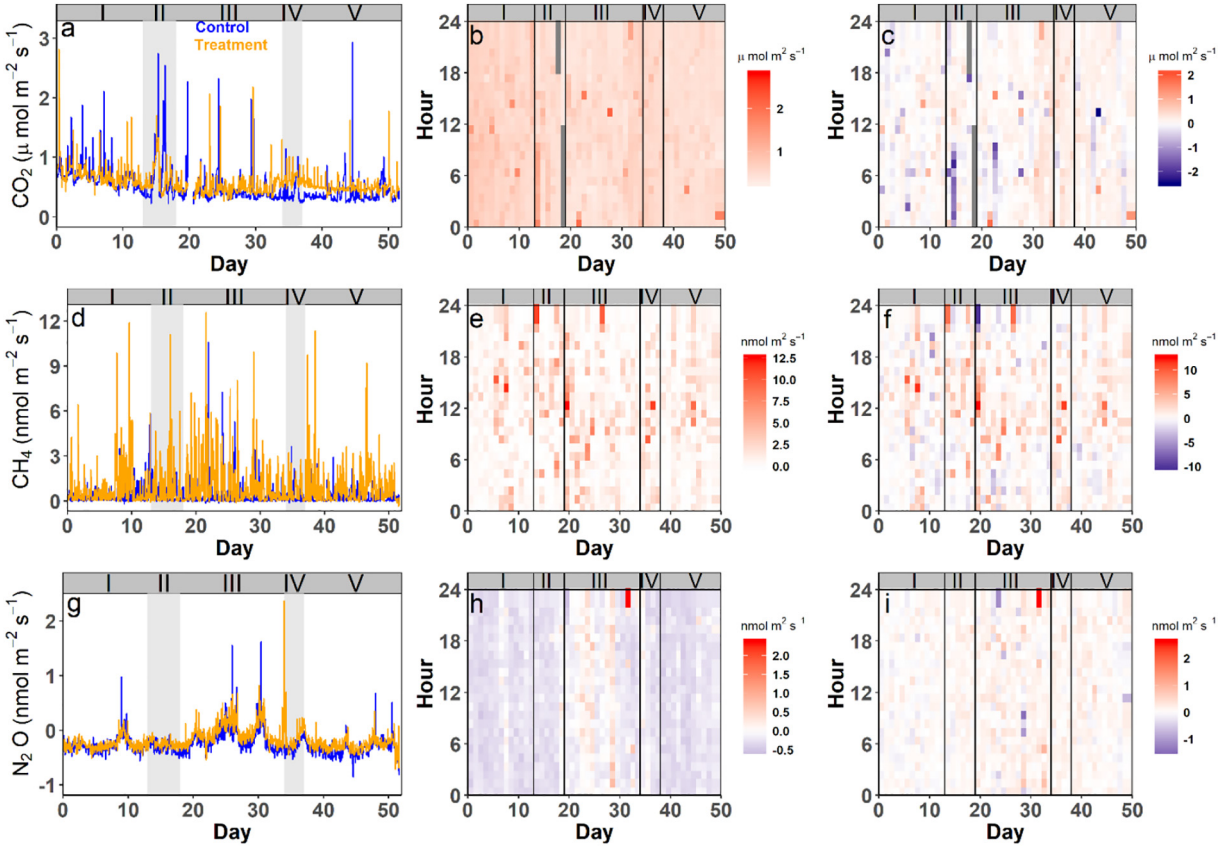

Fig. 2. Averaged hourly time series of CO_2, CH_4, and N_2O, respectively (a, d, g). Heat maps of the hourly fluxes for each GHG gas in the treatment mesocosms (b, e, h). Heat maps of the difference between the treatment and the control (c, f, i). For each heat map, each pixel represents the hourly average (b, e, h) or the difference between the hourly average of the treatment and the control for that day and time (c, f, i).

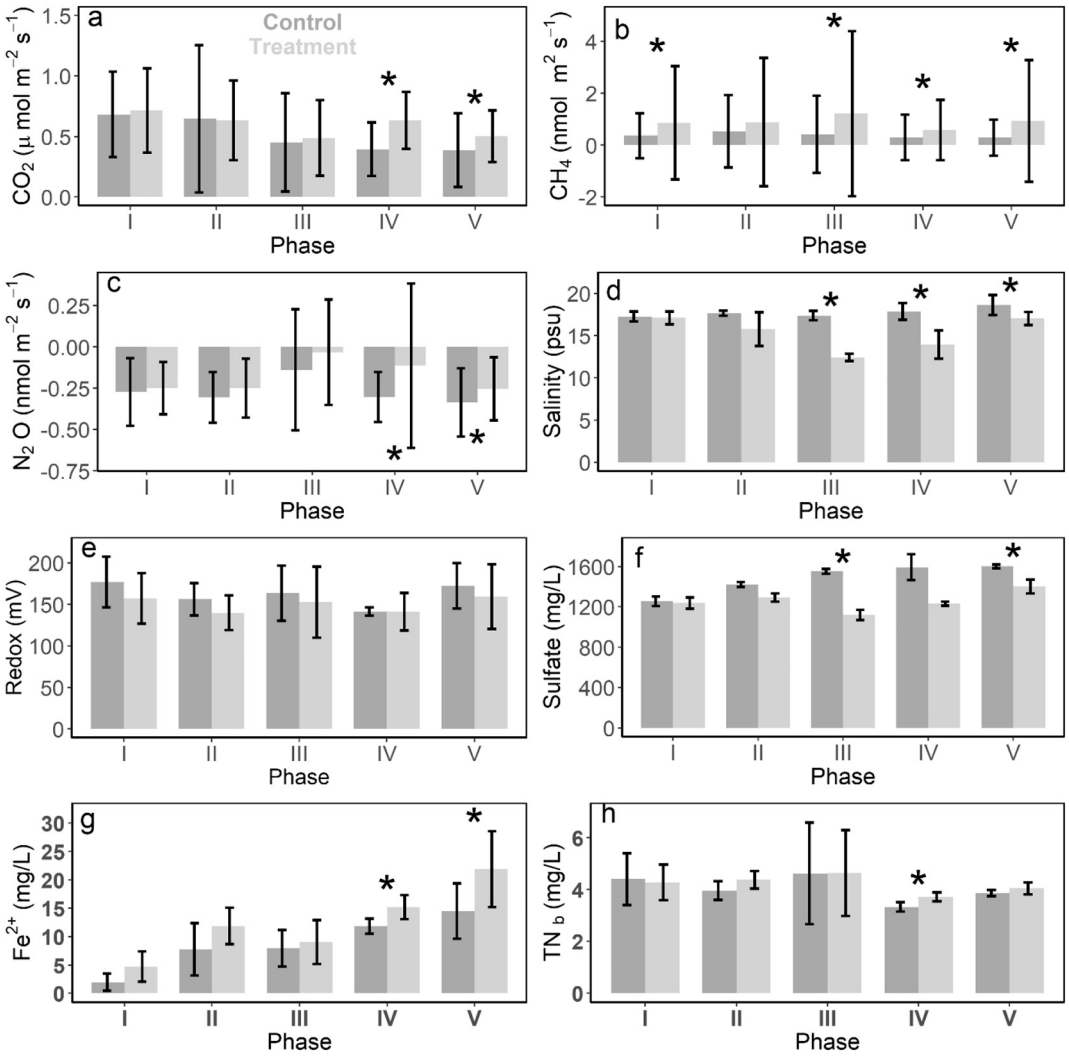

Fig. 3. Bar graphs of the average by phase of the control and treatment of (a) CO_2, (b) CH_4, (c) N_2O, (d) salinity, (e) redox potential, (f) SO_4^{2-}, (g) Fe^2, and (h) TN_b. Error bars represent ±1 SD and asterisks indicate significant differences ($\alpha = 0.05$) between the treatment and the control with the Mann-Whitney *U* test. Dark grey bars represent control and light grey bars treatment results.

3.4. GHG flux hysteresis

We assessed whether the average GHG flux measured at the beginning of the experiment (Phase I) was recovered (or not) by Phase V. For CO_2, there was a clockwise hysteresis effect. The average flux in the beginning was higher than all subsequent phases (Fig. 4a). As the salinity decreased in Phase II and remained low in Phase III, the average CO_2 flux decreased along with it. When the salinity increased in Phase IV, the

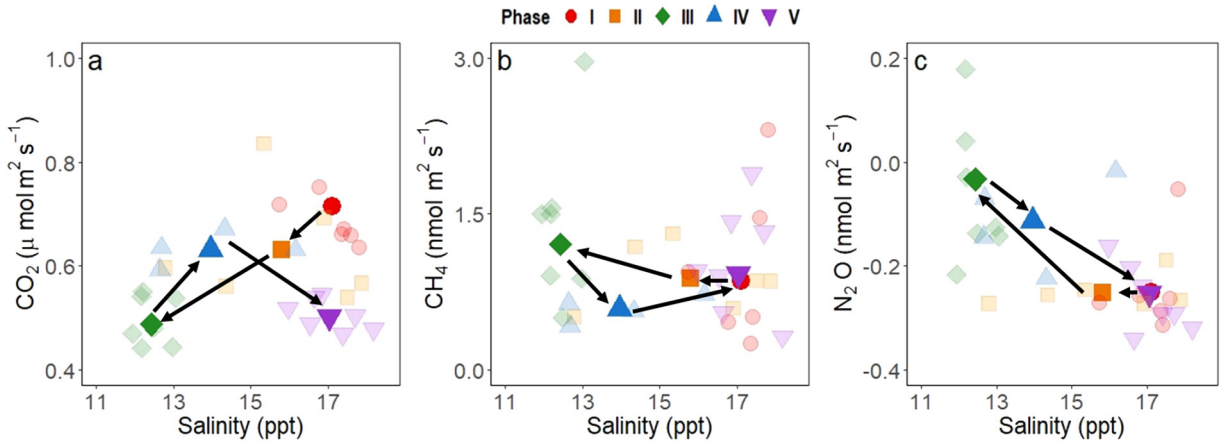

Fig. 4. Hysteresis graphs of (a) CO_2, (b) CH_4, and (c) N_2O for the treatment mesocosms. Arrows indicate the direction of the hysteresis loop. Bolded shapes are the average flux and salinity values for each phase combining all treatment mesocosms. Faded shapes are the daily average flux and salinity values within each phase combining all treatment mesocosms.

fluxes increased as well, and then decreased in Phase V. The average CO_2 fluxes at the beginning and the end of the experiment were significantly different (0.71 ± 0.35 μmol m^{-2} s^{-1} vs 0.50 ± 0.21 μmol m^{-2} s^{-1}).

CH_4 fluxes demonstrated a counter-clockwise hysteresis effect, increasing with decreasing salinity as seen by the increase in the average flux from Phase I to Phase III (Fig. 4b). When salinity increased in Phase IV, the average flux decreased, before increasing slightly in Phase V. The average CH_4 fluxes at the beginning and the end of the experiment were not significantly different (0.86 ± 2.18 nmol m^{-2} s^{-1} vs 0.93 ± 2.35 nmol m^{-2} s^{-1}).

Similar to CO_2, average fluxes of N_2O exhibited a slight clockwise hysteresis loop with N_2O fluxes increasing with decreasing salinity (Phases I - Phase III), before decreasing with an increase in salinity, as seen in the transition from Phase III to Phase V (Fig. 4c). The average N_2O fluxes in the beginning and the end of the experiment were not significantly different (−0.25 ± 0.16 nmol m^{-2} s^{-1} vs −0.25 ± 0.19 nmol m^{-2} s^{-1}).

3.5. Mixed effects models

For all gases, the variables that contributed to the changes in fluxes throughout the experiment differed among phases. Phase I represented conditions before the salinity treatment, no variables were significant because there was no difference between treatment and control collars, and fluxes were stable (i.e., null model was the best model in Phase I for the three gases; Table 1). The mixed effects model for CO_2 during Phase II was not significant, while the model for Phase III showed that variations in redox, along with pH, sulfide, and TN_b explained 49% of the variability in CO_2 fluxes, with pH having the strongest effect. Phase IV was not significant, while Phase V, had 53% of its variability explained by changes in salinity and sulfate. For CH_4, only the model for Phase II was significant. All others (Phases I, III, IV, V) were not significant. For Phase II, pH and sulfide explained 49% of the CH_4 variability. All of the N_2O models were significant (except for Phase I) and explained a large portion of N_2O variability. Sixty-two percent of the variability in N_2O fluxes during Phase II was explained by redox changes. Meanwhile, in Phase III, a variety of parameters contributed to explain 64% of the variation in N_2O flux, with the interaction between sulfate and sulfide having a strong positive effect. During Phase IV, the change in sulfide explained 72% of the flux. Sulfide had a negative relationship with N_2O during this phase. In the final phase of the experiment, redox and salinity contributed to 71% of the variation in N_2O fluxes.

3.6. Global warming potential

Over the duration of the experiment, the treatment mesocosms had higher emissions of CO_2 and CH_4 and were less of a N_2O sink than the control mesocosms (Table 2). The treatment mesocosms have a roughly 24% and 23% higher GWP than the control, for the 20- and 100-year scenarios, respectively.

4. Discussion

We sought to examine the changes in GHG emissions due to dynamic shifts in salinity before, during, and after a storm surge. High frequency measurements of GHG emissions coupled with pore water measurements were used to capture both immediate and temporal trends in GHG fluxes with changes in salinity. Thus, we were able to gain insights into the relative importance of various biogeochemical processes throughout the experiment.

As salinity decreased and remained low during Phases II and III, CO_2 emissions and porewater SO_4^{2-} decreased, while CH_4 emissions

Table 1
Summary of the results of the mixed effect model for each greenhouse gas (CO_2, CH_4, and N_2O) for each phase of the experiment. n.s. = not significant. Averages are reported as mean ± sd.

Model	Variable	Coefficient	SE	t-value	*p*-value
CO_2 – Phase I	n.s.				
CO_2 – Phase II	n.s.				
CO_2 – Phase III *adj.* $R^2 = 0.49$ *P-value* < 0.001	Intercept	−0.38	0.18	−2.17	0.04
	pH	0.58	0.15	3.96	0.0004
	Redox	−0.17	0.09	−1.78	0.09
	Sulfide	0.51	0.20	2.56	0.02
	TN_b	−0.26	0.07	−3.79	0.0007
CO_2 – Phase IV	n.s.				
CO_2 – Phase V	Intercept	−0.26	0.15	−1.78	0.09
adj. $R^2 = 0.53$	Salinity	−0.37	0.17	−2.24	0.03
P-value = 0.008	Sulfate	−0.19	0.10	−1.86	0.07
CH_4 – Phase I	n.s.				
CH_4 – Phase II	Intercept	−0.04	0.21	−0.21	0.84
adj. $R^2 = 0.49$	pH	0.19	0.07	2.82	0.01
P-value = 0.009	Sulfide	0.09	0.06	1.55	0.13
CH_4 – Phase III	n.s.				
CH_4 – Phase IV	n.s.				
CH_4 – Phase V	n.s.				
N_2O – Phase I	n.s.				
N_2O – Phase II	Intercept	−0.37	0.21	−1.77	0.09
adj. $R^2 = 0.62$	Redox	−0.23	0.10	−2.36	0.03
P-value = 0.02					
N_2O – Phase III	Intercept	0.41	0.38	1.08	0.29
adj. $R^2 = 0.64$	Redox	0.37	0.12	2.93	0.01
P-value < 0.001	Sulfate	−0.19	0.21	−0.91	0.37
	Sulfide	0.61	0.25	2.40	0.02
	TN_b	−0.33	0.08	−3.97	0.001
	Salinity	−0.47	0.27	−1.71	0.10
	Sulfate*Sulfide	0.77	0.27	2.86	0.01
N_2O – Phase IV	Intercept	0.20	0.38	0.52	0.61
adj. $R^2 = 0.72$	Sulfide	−1.00	0.20	−5.07	0.0003
P-value < 0.001					
N_2O – Phase V	Intercept	−0.15	0.23	−0.64	0.53
adj. $R^2 = 0.71$	Redox	−0.21	0.06	−3.52	0.002
P-value < 0.001	Salinity	−0.51	0.17	−2.96	0.006

Table 2
The GWP of the control and the treatment cumulative GHG emissions over the entire experiment for 20- and 100-year scenarios.

	CO_2 ($g\ m^{-2}$)	**CH_4** ($CO_{2\text{-eq}}$ ($g\ m^{-2}$))		**N_2O** ($CO_{2\text{-eq}}$ ($g\ m^{-2}$))		**Total** ($CO_{2\text{-eq}}$ ($g\ m^{-2}$))	
	Mean ± SD	20 year GWP scenario	100 year GWP scenario	20 year GWP scenario	100 year GWP scenario	20 year GWP scenario	100 year GWP scenario
Control	99.5 ± 57.1	2.3 ± 5.7	0.90 ± 0.3	−13.8 ± 9.7	−15.3 ± 10.8	88 ± 72.5	85.1 ± 68.2
Treatment	112.6 ± 48.3	5.9 ± 13.4	2.39 ± 5.3	−9.49 ± 11.2	−10.5 ± 12.5	109 ± 72.9	104.4 ± 66.1

increased (Figs. 2a, d, 3a, b, f). A positive relationship between sulfide and CO_2 was found during Phase III. As the supply of SO_4^{2-} declined due to less oceanic water inputs, the amount of sulfide in the pore water increased due to sulfate reduction, releasing CO_2 in the process. At the same time, however, CH_4 emissions increased due to less competition from sulfate reducers (King and Wiebe, 1978), producing CH_4 from CO_2 during the process of methanogenesis and reducing the overall amount of CO_2 emitted from the mesocosms. Subsequently, when salinity increased during Phase IV and stabilized in Phase V, CO_2 emissions increased and CH_4 decreased. As more saline water containing SO_4^{2-} entered the mesocosms, sulfate reduction became more energetically favorable than methanogenesis, resulting in increased CO_2 production and decreased CH_4 production (Capone and Kiene, 1988). During Phase V, there was a near significant negative relationship between CO_2 and SO_4^{2-} as SO_4^{2-} was chemically reduced and more CO_2 was produced (Table 1, Chambers et al., 2013). These results underscore the dynamics between sulfur cycling and CO_2 and CH_4 emissions in tidal salt marsh soils.

Throughout the experiment, GHG emissions, particularly CH_4, were highly variable despite controlled temperature and soil moisture conditions (Fig. 2e). These spikes in CH_4 may be considered hot moments (i.e., short periods of disproportionately high fluxes relative to the time series as a whole (Leon et al., 2014; McClain et al., 2003)). Mechanistically, hot moments occur when all the reactants for a biogeochemical reaction are present at the same time (McClain et al., 2003). The spikes in CH_4 emissions may be due to an unmeasured response to changes in the reactants needed for methanogenesis. However, it is possible that the CH_4 spikes may be the result of ebullition, a known CH_4 transport process in tidal salt marshes and other types of wetlands (Baird et al., 2004; Chanton et al., 1989; Diefenderfer et al., 2018). Similar to Goodrich et al. (2011), we observed ebullition events when the chamber was closed, suggesting that some of the hot moments could be attributed to this process. While CO_2 and N_2O can also experience ebullition, we have not proposed it as a significant gas transport pathway for two reasons: (1) CO_2 and N_2O were not as variable as CH_4 throughout the experiment and (2) previous studies suggest that ebullition does not play a significant role in CO_2 and N_2O transport (Gao et al., 2013; Komiya et al., 2015; Tuser et al., 2017). The variability present in CH_4 and to a lesser degree in CO_2 and N_2O, highlights the importance of high-frequency measurements in both field and lab settings in order to accurately capture the dynamics of GHG emissions.

For the majority of the experiment, the soils were sinks of N_2O (Fig. 2g, h). There have been reported instances of N_2O sinks in wetlands (Audet et al., 2014; Minami, 1997; Reddy and Delaune, 2008; Ryden, 1981; Slemr and Seiler, 1984). Diefenderfer et al. also found negative fluxes of N_2O in a *Sarcocornia* marsh during a storm surge (2018); however, the mechanisms behind N_2O consumption in salt marshes are not well-understood (Chapuis-Lardy et al., 2007). The soils in our experiments remained flooded, likely increasing N_2O consumption due to the lower diffusivity rate in water and the increased residence time of the gas (Arah et al., 1991). Generally, N_2O consumption occurs in soils with a high water-filled pore space and low NO_3^- availability (Clayton et al., 1997; Khalil et al., 2002; Ryden, 1983; Wagner-Riddle et al., 1997), which was the case during our experiment. Under these conditions, it is possible that some of the N_2O consumption could be attributed to N_2O serving as electron acceptor for denitrification (Butterbach-Bahl et al., 1998; Goossens et al., 2001; Rosenkranz et al., 2006). The persistence of the N_2O sink for all mesocosms raises questions about the potential of salt marsh soils to become sinks during storm surges or in sea level rise scenarios and how this capability could offset increased CO_2 and CH_4 emissions during periods of decreased salinity.

Redox and redox-sensitive ions and compounds likely affected N_2O fluxes. During Phase II, redox had a negative relationship with N_2O. Both the control and the treatment soils were lower than the N_2O reduction critical redox potential of 250 mV (Letey et al., 1981; Smith et al., 1983; Yu and Patrick, 2003). However, as the salinity remained stable in Phase III, redox had a significant, positive relationship with N_2O. As treatment redox increased towards the N_2O reduction critical redox potential, the soils became less of a sink. Furthermore, the significant, negative relationship between TN_b and N_2O, suggests that nitrogen compounds were being consumed to produce N_2O. As the salinity increased, sulfide had a significant, negative relationship with N_2O. Though not much research has been done on the effect of sulfides on N_2O emission in wetlands, it may be that the presence of sulfides, a by-product of sulfate reduction, indicates that the system shifted from nitrate reduction to sulfate reduction.

Hysteresis graphs were used to assess the functional response of changes in salinity over the course of the experiment (Phillips et al., 2011; Riveros-Iregui et al., 2007; Vargas and Allen, 2008). All GHG showed hysteresis effects, though N_2O had only a slight hysteresis. CH_4 and N_2O had near-identical final and initial fluxes, which suggests that the potential processes that influence CH_4 and N_2O efflux had fully recovered within 15 days, illustrating the resiliency of tidal salt marsh soils to pulse events. A previous study done by Northrup et al. (2018) found that the in situ increase in As concentration during Hurricane Joaquin at our study site had returned to baseline concentrations within 1 week of the event, suggesting that the biogeochemical conditions (e.g. pH, redox) at the site had recovered quickly. The presence of hysteresis may be the result of differences in the rates of biogeochemical pathways due to changing quantities of reactants and inhibitors throughout the experiment. Hysteresis effects on GHG efflux due to salinity changes could be incorporated into modelling efforts since there is a non-linear response that increases or decreases the overall GHG efflux from the pulse event.

Overall, the simulated decrease in salinity caused by a hurricane-induced surge increased the 20- and 100-year GWP of the mesocosms. This increase in GWP from treatment mesocosms was mainly due to higher CH_4 fluxes, but these higher CH_4 fluxes were slightly offset by N_2O consumption. The strength of the N_2O sink was weaker in the treatment mesocosms compared to the control. These results prompt questions about processes that govern N_2O sinks (i.e., when do they occur and how do they change under different scenarios). Additionally, our results raise questions about the effect of sea level rise and its accompanying increase in salinity (mainly as sulfate) on GHG fluxes, as our data indicate that sea level rise could decrease CH_4 emissions from wetland soils. These processes should be explored in future research.

5. Conclusions

By combining high temporal frequency measurements of CO_2, CH_4, and N_2O with pore water chemistry, we were able to better understand

how shifts in potential biogeochemical pathways, such as sulfate reduction, could impact GHG emissions. We found that efflux can be highly variable, especially for CH_4, despite controlling for confounding effects such as water level and temperature. This underscores the need to take continuous, high-frequency data in the field in order to capture the variability. Furthermore, we found that decreased salinity does increase GHG emissions under flooded conditions, and that the biogeochemical processes by which it does appears to continually evolve, with different electron acceptors playing roles at different times during the experiment. Overall, the lowered salinity in the treatment soils produced a 24% and 23% increase in GWP under 20- and 100-year scenarios, respectively, suggesting that pulse events can cause a burst of GHG emissions from tidal salt marsh soils. However, it is important to note that when initial conditions were restored, CH_4 and N_2O emissions returned to baseline within 15 days, likely by different pathways. Overall, the experimental results suggest that tidal salt marshes are resilient ecosystems that can recover from disturbances relatively quickly, but raises questions about the effects of increasing salinity (i.e. sea level rise) on GHG fluxes from tidal marshes.

Declaration of Competing Interest

The authors declare no conflict of interest.

Acknowledgements

MC acknowledges support from a DENIN Environmental Fellowship, as well as a National Science Foundation Graduate Research Fellowship (#1247394), RV acknowledges support from the National Science Foundation (#1652594), and ALS acknowledges support from the National Science Foundation (#175987). We thank the support from the staff at St. Jones Reserve, as well as the staff at the University of Delaware Soil Testing Lab.

Author contributions

MC, JB, ALS and RV designed the experiment. MC performed the experiment, analyzed data, and wrote the manuscript with input from all coauthors.

Appendix A. Supplementary data

Supplementary data to this article can be found online at https://doi.org/10.1016/j.scitotenv.2019.06.032.

References

Arah, J.R.M., Smith, K.A., Crichton, I.J., Li, H.S., 1991. Nitrous oxide production and denitrification in Scottish arable soils. J. Soil Sci. 42, 351–367. https://doi.org/10.1111/j.1365-2389.1991.tb00414.x.

Audet, J., Hoffmann, C.C., Andersen, P.M., Baattrup-Pedersen, A., Johansen, J.R., Larsen, S.E., Kjaergaard, C., Elsgaard, L., 2014. Nitrous oxide fluxes in undisturbed riparian wetlands located in agricultural catchments: emission, uptake and controlling factors. Soil Biol. Biochem. 68, 291–299. https://doi.org/10.1016/j.soilbio.2013.10.011.

Baird, A.J., Beckwith, C.W., Waldron, S., Waddington, J.M., 2004. Ebullition of methane-containing gas bubbles from near-surface Sphagnum peat. Geophys. Res. Lett. 31, 2–5. https://doi.org/10.1029/2004GL021157.

Barton, K., 2018. MuMIn: Multi-Model Inference.

Bridgham, S.D., Megonigal, J.P., Keller, J.K., Bliss, N.B., Trettin, C., 2006. The carbon balance of north American wetlands. Wetlands 26, 889–916. https://doi.org/10.1672/0277-5212(2006)26[889:tcbona]2.0.co;2.

Butterbach-Bahl, K., Gasche, R., Huber, C., Kreutzer, K., Papen, H., 1998. Impact of N-input by wet deposition on N-trace gas fluxes and CH_4-oxidation in spruce forest ecosystems of the temperate zone in Europe. Atmos. Environ. 32, 559–564. https://doi.org/10.1016/S1352-2310(97)00234-3.

Capone, D.G., Kiene, R.P., 1988. Comparison of microbial dynamics in marine and freshwater sediment. Limnol. Ocean. 33, 725–749.

Chambers, L.G., Osborne, T.Z., Reddy, K.R., 2013. Effect of salinity-altering pulsing events on soil organic carbon loss along an intertidal wetland gradient: a laboratory experiment. Biogeochemistry 115, 363–383. https://doi.org/10.1007/s10533-013-9841-5.

Chanton, J.P., Martens, C.S., Kelley, C.A., 1989. Gas transport from methane-saturated, tidal freshwater and wetland sediments. Limnol. Oceanogr. 34, 807–819. https://doi.org/10.4319/lo.1989.34.5.0807.

Chapuis-Lardy, L., Wrage, N., Metay, A., Chotte, J.-L., Bernoux, M., 2007. Soils, a sink for N_2O? A review. Glob. Biogeochem. Cycles 13, 1–17. https://doi.org/10.1111/j.1365-2486.2006.01280.x.

Clayton, H., McTaggart, I.P., Parker, J., Swan, L., Smith, K.A., 1997. Nitrous oxide emissions from fertilised grassland: a 2-year study of the effects of N fertiliser form and environmental conditions. Biol. Fertil. Soils 25, 252–260.

Clough, T.J., Sherlock, R.R., Rolston, D.E., 2005. A review of the movement and fate of N_2O in the subsoil. Nutr. Cycl. Agroecosystems 72, 3–11. https://doi.org/10.1007/s10705-004-7349-z.

Crooks, S., Herr, D., Tamelander, J., Laffoley, D., Vandever, J., 2011. Mitigating climate change through restoration and Management of Coastal Wetlands and Near-Shore Marine Ecosystems: Challenges and opportunities, Environmen. Environment Department Paper. World Bank, Washington D.C.

Dahl, T.E., 2011. Status and Trends of Wetlands in the Conterminous United States 2004 to 2009. U.S. Dep. Inter. Fish Wildl. Serv, p. 108.

Dahl, T.E., Stedman, S.M., 2013. Status and Trends of Wetlands in the Coastal Watersheds of the Conterminous United States 2004 to 2009.

Davidson, E.A., 1991. Fluxes of nitrous oxide and nitric oxide from terrestrial ecosystems. In: Rogers, J.E., Whitman, W.B. (Eds.), Microbial Production and Consumption of Greenhouse Gases: Methane, Nitrogen Oxides, and Halomethanes. American Society of Microbiology, Washington D.C., pp. 219–235.

Diefenderfer, H.L., Cullinan, V.I., Borde, A.B., Gunn, C.M., Thom, R.M., 2018. High-frequency greenhouse gas flux measurement system detects winter storm surge effects on salt marsh. Glob. Chang. Biol. 24, 5961–5971. https://doi.org/10.1111/gcb.14430.

DNREC, 1999. Delaware National Esturaine Research Reserve Estuarine Profile.

Forster, P., Ramaswany, V., Artaxo, P., Berntsen, T., Betts, R., Fahey, D.W., Haywood, J., Lean, J., Lowe, D.C., Myhre, G., Nganga, J., Prinn, R., Raga, G., Schulz, M., Van Dorland, R., 2007. Changes in atmospheric constituents and in radiative forcing. In: Solomon, S., Qin, D., Manning, M., Chen, Z., Marquis, M., Averyt, K.B., Tignor, M., Miller, H.L. (Eds.), Climate Change 2007: The Physical Science Basis. Contribution of Working Group I to the Fourth Assessment Report of the Intergovernmental Panel on Climate Change. Cambridge, UK, pp. 129–234 https://doi.org/10.1103/PhysRevB.77.220407.

Furukawa, Y., Smith, A.C., Kostka, J.E., Watkins, J., Alexander, C.R., Dava Dalton, A., Vaughan, C., Dollhopf, S., Dollhopf, M., Skelton, H., Petrie, L., Adams, H., 2004. Quantification of macrobenthic effects on diagenesis using a multicomponent inverse model in salt marsh sediments. Limnol. Ocean. 49, 2058–2072.

Gao, Y., Liu, X., Yi, N., Wang, Y., Guo, J., Zhang, Z., Yan, S., 2013. Estimation of N_2 and N_2O ebullition from eutrophic water using an improved bubble trap device. Ecol. Eng. 57, 403–412. https://doi.org/10.1016/J.ECOLENG.2013.04.020.

Gelman, A., Hill, J., 2007. Data Analysis Using Regression and Multilevel/Hierarchical Models. 1st ed. Cambridge University Press, Cambridge, UK.

Goodrich, J.P., Varner, R.K., Frolking, S., Duncan, B.N., Crill, P.M., 2011. High-frequency measurements of methane ebullition over a growing season at a temperate peatland site. Geophys. Res. Lett. 38. https://doi.org/10.1029/2011GL046915 n/a-n/a.

Goossens, A., De Visscher, A., Boeckx, P., Cleemput, O. Van, 2001. Two-year field study on the emission of N_2O from coarse and middle-textured Belgian soils with different land use. Nutr. Cycl. Agroecosyst. 60 (1-3), 23–34.

Heincke, M., Kaupenjohann, M., 1999. Effects of soil solution on the dynamics of N2O emissions: a review. Nutr. Cycl. Agroecosystems 55, 133–157.

Inubushi, K., Barahona, M.A., Yamakawa, K., 1999. Effects of salts and moisture content on N_2O emission and nitrogen dynamics in yellow soil and andosol in model experiments. Biol. Fertil. Soils 29, 401–407.

IPCC, 2000. Land Use, Land-Use Change, and Forestry: Summary for Policymakers.

IPCC, 2014. Climate Change 2014: Synthesis Report. Contribution of Working Groups I, II and III to the Fifth Assessment Report of the Intergovernmental Panel on Climate Change. Geneva, Switzerland. https://doi.org/10.1017/CBO9781107415324.004.

Jordan, S.J., Stoffer, J., Nestlerode, J.A., 2011. Wetlands as sinks for reactive nitrogen at continental and global scales: a meta-analysis. Ecosystems 14, 144–155.

Jørgensen, C.J., Elberling, B., 2012. Effects of flooding-induced N_2O production, consumption and emission dynamics on the annual N_2O emission budget in wetland soil. Soil Biol. Biochem. 53, 9–17. https://doi.org/10.1016/j.soilbio.2012.05.005.

Khalil, M.I., Rosenani, A.B., Van Cleemput, O., Fauziah, C.I., Shamshuddin, J., 2002. Nitrous oxide emissions from an Ultisol of the humid tropics under maize–groundnut rotation. J. Environ. Qual. 31, 1071. https://doi.org/10.2134/jeq2002.1071.

King, G.M., Wiebe, W.J., 1978. Methane Release From Soils of a Georgia Salt Marsh. 42 (343–10).

Kliewer, B.A., Gilliam, J.W., 1995. Water table management effects on denitrification and nitrous oxide evolution. Soil Sci. Soc. Am. J. 59, 1694. https://doi.org/10.2136/sssaj1995.03615995005900060027x.

Komiya, S., Noborio, K., Katano, K., Pakoktom, T., Siangliw, M., Toojinda, T., 2015. Contribution of ebullition to methane and carbon dioxide emission from water between plant rows in a tropical Rice Paddy Field. Int. Sch. Res. Not. 2015, 1–8. https://doi.org/10.1155/2015/623901.

Leon, E., Vargas, R., Bullock, S., Lopez, E., Panosso, A.R., La Scala, N., 2014. Hot spots, hot moments, and spatio-temporal controls on soil CO_2 efflux in a water-limited ecosystem. Soil Biol. Biochem. 77, 12–21. https://doi.org/10.1016/J.SOILBIO.2014.05.029.

Letey, J., Valoras, N., Focht, D.D., Ryden, J.C., 1981. Nitrous oxide production and reduction during denitrification as affected by redox potential. Soil Sci. Soc. Am. J. 45, 727–730. https://doi.org/10.2136/sssaj1981.03615995004500040010x.

Liikanen, A., Martikainen, P.J., 2003. Effect of ammonium and oxygen on methane and nitrous oxide fluxes across sediment-water interface in a eutrophic lake. Chemosphere 52, 1287–1293. https://doi.org/10.1016/S0045-6535(03)00224-8.

Martikainen, P.J., Nykanen, H., Crill, P., Silvola, J., 1993. Effects of a lowered water table on nitrous oxide fluxes from northern peatlands. Nature 366.
McClain, M.E., Boyer, E.W., Dent, C.L., Gergel, S.E., Grimm, N.B., Groffman, P.M., Hart, S.C., Harvey, J.W., Johnston, C.A., Mayorga, E., Mcdowell, W.H., Pinay, G., 2003. Biogeochemical hot spots and hot moments at the interface of terrestrial and aquatic ecosystems. Ecosystems 6, 301–312. https://doi.org/10.1007/s10021-003-0161-9.
McLeod, E., Chmura, G.L., Bouillon, S., Salm, R., Björk, M., Duarte, C.M., Lovelock, C.E., Schlesinger, W.H., Silliman, B.R., 2011. A blueprint for blue carbon: toward an improved understanding of the role of vegetated coastal habitats in sequestering CO_2. Front. Ecol. Environ. 9, 552–560. https://doi.org/10.1890/110004.
Menyailo, O., Stepanov, A., Umarov, M.M., 1997. The transformation of nitrous oxide by denitrifying bacteria in Solonchaks. Eurasian Soil Sci 30, 178–180.
Minami, K., 1997. Atmospheric methane and nitrous oxide: sources, sinks and strategies for reducing agricultural emissions. Nutr. Cycl. Agroecosystems 49, 203–211.
Myhre, G., Shindell, D., Bréon, F.-M., Collins, W., Fuglestvedt, J., Huang, J., Koch, D., Lamarque, J.-F., Lee, D., Mendoza, B., Nakajima, T., Robock, A., Stephens, G., Takemura, T., Zhang, H., Qin, D., Plattner, G., Tignor, M., Allen, S., Boschung, J., Nauels, A., Xia, Y., Bex, V., Midgley, P., 2013. Anthropogenic and natural radiative forcing. Climate Change 2013: The Physical Science Basis. Contribution of Working Group I.
NOAA National Estuarine Research Reserve System (NERRS), 2015. System-Wide Monitoring Program. WWW Document. NOAA NERRS Cent. Data Manag. Off.
Northrup, K., Capooci, M., Seyfferth, A.L., 2018. Effects of extreme events on arsenic cycling in salt marshes. J. Geophys. Res. Biogeosci. 123, 1086–1100. https://doi.org/10.1002/2017JG004259.
Petrakis, S., Barba, J., Bond-Lamberty, B., Vargas, R., 2017a. Using greenhouse gas fluxes to define soil functional types. Plant Soil https://doi.org/10.1007/s11104-017-3506-4.
Petrakis, S., Seyfferth, A., Kan, J., Inamdar, S., Vargas, R., 2017b. Influence of experimental extreme water pulses on greenhouse gas emissions from soils. Biogeochemistry 133, 147–164. https://doi.org/10.1007/s10533-017-0320-2.
Phillips, C.L., Nickerson, N., Risk, D., Bond, B.J., 2011. Interpreting diel hysteresis between soil respiration and temperature. Glob. Chang. Biol. 17, 515–527. https://doi.org/10.1111/j.1365-2486.2010.02250.x.
Pinheiro, J., Bates, D., DebRoy, S., Sarkar, D., R Core Team, 2018. Nlme: Linear and Nonlinear Mixed Effects Models.
Poffenbarger, H.J., Needelman, A., Megonigal, J.P., 2011. Salinity influence on methane emissions from tidal marshes. Wetlands https://doi.org/10.1007/s13157-011-0197-0.
Ponnamperuma, F.N., 1972. The chemistry of submerged soils. Adv. Agron. 24, 29–96.
Reddy, K.R., Delaune, R.D., 2008. Biogeochemistry of Wetlands: Science and Applications. CRC Press, Boca Ration, FL.
Riveros-Iregui, D.A., Emanuel, R.E., Muth, D.J., McGlynn, B.L., Epstein, H.E., Welsch, D.L., Pacific, V.J., Wraith, J.M., 2007. Diurnal hysteresis between soil CO_2 and soil temperature is controlled by soil water content. Geophys. Res. Lett. 34, 1–5. https://doi.org/10.1029/2007GL030938.
Rosenkranz, P., Brüggemann, N., Brüggemann, B., Papen, H., Xu, Z., Seufert, G., Butterbach-Bahl, K., 2006. N2O, NO and CH4 exchange, and microbial N turnover over a Mediterranean pine forest soil. Biogeosciences 3, 121–133.
Ryden, J.C., 1981. N_2O exchange between a grassland soil and the atmosphere. Nature 292, 235–237. https://doi.org/10.1038/292235a0.
Ryden, J.C., 1983. Denitrification loss from a grassland soil in the field receiving different rates of nitrogen as ammonium nitrate. J. Soil Sci. 34, 355–365. https://doi.org/10.1111/j.1365-2389.1983.tb01041.x.
Schaufler, G., Kitzler, B., Schindlbacher, A., Skiba, U., Sutton, M.A., Zechmeister-Boltenstern, S., 2010. Greenhouse gas emissions from European soils under different land use: effects of soil moisture and temperature. Eur. J. Soil Sci. 61, 683–696. https://doi.org/10.1111/j.1365-2389.2010.01277.x.
Seyfferth, A.L., Fendorf, S., 2012. Silicate Mineral Impacts on the Uptake and Storage of Arsenic and Plant Nutrients in Rice (*Oryza sativa* L.). https://doi.org/10.1021/es3025337.
Slemr, F., Seiler, W., 1984. Field measurements of NO and NO_2 emissions from fertilized and unfertilized soils. J. Atmos. Chem. 2, 1–24. https://doi.org/10.1007/BF00127260.
Smith, C.J., DeLaune, R.D., Patrick, J.W.H., 1983. Nitrous oxide emission from Gulf Coast wetlands. Geochim. Cosmochim. Acta 47, 1805–1814. https://doi.org/10.1016/0016-7037(83)90028-5.
Tobias, C., Neubauer, S.C., 2019. Salt marsh biogeochemistry – An overview. Coastal Wetlands: An Integrated Ecosystem Approach, pp. 445–492.
Tuser, M., Picek, T., Sajdlov, Z., Jůza, T., Muska, M., Frouzov, J., 2017. Seasonal and spatial dynamics of gas ebullition in a temperate water-storage reservoir. Water Resour. Res. 53, 8266–8276. https://doi.org/10.1002/2017WR020694.
Valiela, I., Teal, J.M., 1979. The nitrogen budget of a salt marsh ecosystem. Nature 280, 652–656. https://doi.org/10.1038/280652a0.
Vargas, R., Allen, M.F., 2008. Diel patterns of soil respiration in a tropical forest after hurricane Wilma. J. Geophys. Res. Biogeosci. 113, 1–10. https://doi.org/10.1029/2007JG000620.
Wagner-Riddle, C., Thurtell, G.W., Kidd, G.K., Beauchamp, E.G., Sweetman, R., 1997. Estimates of nitrous oxide emissions from agricultural fields over 28 months. Can. J. Soil Sci. 77, 135–144.
Wong, P.P., Losanda, I.J., Gattuso, J.-P., Hinkel, J., Khattabi, A., McInnes, K.L., Saito, Y., Sallenger, A., 2014. Coastal systems and low-lying areas. In: Field, C.B., Barros, V.R., Dokken, D.J., Mach, K.J., Mastrandrea, M.D., Bilir, T.E., Chatterjee, M., Ebi, K.L., Estrada, Y.O., Genova, R.C., Girma, B., Kissel, E.S., Levy, A.N., MacCracken, S., Mastrandrea, P.R., White, L.L. (Eds.), Climate Change 2014: Impacts, Adaptation, and Vulnerability. Part a: Global and Sectoral Aspects. Contribution of Working Group II to the Fifth Assessment Report of the Intergovernmental Panel on Climate Change. Cambridge University Press, Cambridge, UK, pp. 361–409.
Yu, K., Patrick, W.H., 2003. Redox range with minimum nitrous oxide and methane production in a rice soil under different pH. Soil Sci. Soc. Am. J. 67, 1952. https://doi.org/10.2136/sssaj2003.1952.
Zuur, A.F., Ieno, E.N., Elphick, C.S., 2010. A protocol for data exploration to avoid common statistical problems. Methods Ecol. Evol. 1, 3–14. https://doi.org/10.1111/j.2041-210X.2009.00001.x.